A New Algorithm for Multicomponent Signals Analysis Based on SynchroSqueezing: With an Application to Signal Sampling and Denoising

Sylvain Meignen
IDCOM Laboratory,
University of Edinburgh Scotland, UK
Tel:0044-131-650-5659
email: sylvain.meignen@imag.fr
Thomas Oberlin
Jean Kuntzmann Laboratory,
University of Grenoble, France
Tel:0033-4-76-51-45-61
email: thomas.oberlin@imag.fr
Steve McLaughlin FIEEE,
School of Engineering and Physical Sciences,
Heriot-Watt University, Edinburgh Scotland, UK
Tel 0044 131 451 4127
email: s.mclaughlin@hw.ac.uk

Abstract- In this paper, we address the problem of the retrieval of the components from a multicomponent signal using ideas from the synchrosqueezing framework. The emphasis is on the wavelet choice and we propose a novel algorithm based first on the detection of components followed by their reconstruction. Simulations illustrate how the proposed procedure compares with the empirical mode decomposition and other related methods in terms of mode-mixing. We conclude the paper by studying the sensitivity of the proposed technique to sampling and an application to signal denoising.

Keywords-SynchroSqueezing, Wavelets, EMD, Time-Frequency, Sampling, Denoising
EDICS Category: DSP-TFSR

I. Introduction

Audio signals are commonly modelled as a sum of AM/FM components with slowly varying amplitude and instantaneous frequency [19]. Consequently, the retrieval of the components (or modes) of a multicomponent signal (RCM) is a central issue in many audio processing problems. The most commonly used techniques to carry out theretrieval are time-frequency or time-scale based signal representations. For the former, spectrogram reassignment techniques [4], reconstruction based on l_1 minimization of the ambiguity function associated with the Wigner-Ville distribution [7], synchrosqueezing using the short time Fourier transform [20] or Fourier ridges [3] have all been successfully used. For the latter, i.e., time-scale representations, wavelet ridges have also proven to be very efficient [14] [13]. In [13], the emphasis is on the importance of the wavelet choice with regard to the ridge representation. Synchrosqueezing techniques have also been developed within the wavelet framework [5]. The main difference between the short time Fourier and wavelet representations is that the latter is more demanding in terms of the frequency separation of high frequency components.

In this paper, we first propose a new implementation for the RCM following on from some ideas of the synchrosqueezing transform (SST) and then show how it enables us to find out a relevant non-uniform sampling set for the signal, i.e., preserving its essential frequency characteristics, and finally how it can be used for signal denoising. The layout of the paper is as follows. In section II, we recall some notation that is useful to describe the SST and then restate the main theoretical related results [5] with a practical implementation of the RCM recently proposed by Brevdo et *al.* in [1] (section II-D). A fundamental issue in synchrosqueezing-based methods is the mother wavelet choice ; a poor wavelet representation inevitably leads to a poor SST result. Therefore, in section III, we focus on the difference between wavelet transforms of pure harmonic and of multicomponent signals. We deduce from this study that a good wavelet representation for a sum of pure harmonic signals only requires that the mother wavelet fulfills an appropriate *separation condition* while for more general multicomponent signals the mother wavelet choice must also take into account the *modulation parameter* associated with the different components. Bearing in mind these elements, we propose a new implementation of the RCM in section IV-C. It is based on an automatic mode detection step followed by a reconstruction step that takes into account the particular structure of the wavelet transform of multicomponent signals. The numerical simulations of section V show that the proposed reconstruction algorithm provides good mode separation and compares favorably to *empirical mode decomposition* (EMD) [11] and another existing RCM algorithm related to the SST [1]. Finally, we conclude the paper by proposing a potential use of the proposed RCM technique

for efficient sampling and denoising of multicomponent signals.

II. Synchrosqueezing Basis

A. Notation

We denote by $\hat{f}$ the Fourier transform of f, defined using the following normalization:

$$\hat{f}(\xi) = \int_{\mathbb{R}} f(x) e^{-2i\pi\xi x} dx. \tag{1}$$

For $f \in L^2(\mathbb{R})$, we define the continuous wavelet transform (WT):

$$W_f(a,t) = \int_{\mathbb{R}} f(x) \frac{1}{a} \overline{\Psi(\frac{x-t}{a})} dx, \tag{2}$$

where $\Psi \in L^2(\mathbb{R})$ is a function called mother wavelet satisfying the condition $\int_0^{+\infty} \frac{\left|\hat{\Psi}(\xi)\right|^2}{\xi} d\xi < +\infty$. It is said to be analytic if $\hat{\Psi}(\xi) = 0$, $\xi \leq 0$. A particular class of analytic wavelets are those admitting a unique peak frequency ξ_Ψ defined by:

$$\xi_\Psi := \operatorname*{argmax}_\xi \left|\hat{\Psi}(\xi)\right|. \tag{3}$$

As an illustration, consider the *bump wavelet* defined

$$\hat{\Psi}(\xi) = e^{1 - \frac{1}{1-(\frac{\xi-\mu}{\sigma})^2}} \chi_{[\mu-\sigma,\mu+\sigma]}, \tag{4}$$

which admits the peak frequency $\xi_\Psi = \mu$ and where χ_I is the indicator function of the set I.

B. Problem Setting

In what follows, we investigate the retrieval of the components f_k of a multicomponent signal f defined by:

$$f(t) = \sum_{k=1}^{K} A_k(t) \cos(2\pi\phi_k(t)) = \sum_{k=1}^{K} f_k(t), \tag{5}$$

where $A_k(t) > 0$ and $\phi_k'(t) > 0$. The problem can be viewed from two perspectives. The first consists of computing an approximation of the modes, either by using EMD [11] or via wavelet projections [17]. The second [1] uses the SST to reallocate the WT before proceeding with multicomponent retrieval.

C. Theoretical Aspects of the SST

For the sake of consistency, we recall some theoretical results stated in [5]. These were established for a signal f defined as a superposition of *intrinsic-mode-type* functions (IMT):

Definition 1: A continuous function $f : \mathbb{R} \to \mathbb{R} \in L^\infty(\mathbb{R})$ is said to be of the *intrinsic-mode-type (IMT) with accuracy* ϵ (or ϵ-IMT) if $f(t) = A(t)\cos(2\pi\phi(t))$ with A and ϕ satisfying the following properties:

$$\begin{array}{l} A \in C^1(\mathbb{R}) \bigcap L^\infty(\mathbb{R}),\ \phi \in C^2(\mathbb{R}) \\ \\ \inf\limits_{t\in\mathbb{R}} \phi'(t) > 0,\ \sup\limits_{t\in\mathbb{R}} \phi'(t) < \infty,\ \sup\limits_{t\in\mathbb{R}} |\phi''(t)| < \infty \\ |A'(t)|, |\phi''(t)| \leq \epsilon |\phi'(t)|,\ \forall t \in \mathbb{R} \end{array}$$

Definition 2: A function $f : \mathbb{R} \to \mathbb{R}$ is said to be a superposition of well-separated ϵ-IMTs with separation d, the set of which is denoted by $\mathcal{A}_{\epsilon,d}$ in the sequel, if there exists a finite K such that $f(t) = \sum\limits_{k=1}^{K} f_k(t) = \sum\limits_{k=1}^{K} A_k(t)\cos(2\pi\phi_k(t))$, where all the f_k are ϵ-IMTs satisfying:

$$\left\{ \begin{array}{l} \phi_k'(t) > \phi_{k-1}'(t) \\ \\ |\phi_k'(t) - \phi_{k-1}'(t)| \geq d(\phi_{k-1}'(t) + \phi_k'(t)). \end{array} \right.$$

In the following, the condition involving d will be called the *separation condition*. Consider the following description of the frequency representation of f in the time-scale space:

$$\hat{\omega}(a,t) \quad = \quad \frac{\partial_t W_f(a,t)}{2i\pi W_f(a,t)}, \tag{6}$$

which is only defined for a non zero wavelet coefficient. The main theorem defining the SST was detailed in [5] and is:

Theorem 1: Let f be a function in $\mathcal{A}_{\epsilon,d}$ and set $\tilde{\epsilon} = \epsilon^{1/3}$. Select a function h in C_c^∞ and a mother wavelet Ψ in the Schwartz class such that $\hat{\Psi}$ is supported in $[\xi_\Psi - \Delta, \xi_\Psi + \Delta]$, with $\Delta < d\xi_\Psi/(1+d)$. Consider the function obtained by synchrosqueezing W_f, with threshold $\tilde{\epsilon}$ and accuracy α, i.e.

$$S_{f,\tilde{\epsilon}}^{\alpha}(\omega,t) = \int_{A_{\tilde{\epsilon},f}(t)} W_f(a,t)\frac{1}{\alpha}h(\frac{|\omega - \hat{\omega}(a,t)|}{\alpha})\frac{da}{a},$$

where $A_{\tilde{\epsilon},f}(t) = \{a \in \mathbb{R}^+; |W_f(a,t)| > \tilde{\epsilon}\}$. Then provided ϵ is sufficiently small, the following conditions hold:

- $|W_f(a,t)| > \tilde{\epsilon}$ only when for some $k \in \{1, \cdots, K\}$, $(a,t) \in Z_k := \{(a,t); |a\phi_k'(t) - \xi_\Psi| < \Delta\}$.
- For each $k \in \{1, \cdots, K\}$, and for each pair $(a,t) \in Z_k$, for which holds $|W_f(a,t)| > \tilde{\epsilon}$, we have $|\hat{\omega}(a,t) - \phi_k'(t)| \leq \tilde{\epsilon}$
- Moreover, for each $k \in \{1, \cdots, K\}$, there exists a constant C, such that, for any t in $\mathbb{R}$,

$\left|\lim_{\alpha\to 0}\frac{2}{C_\Psi}\mathcal{R}e\left[\int_{B_{\tilde{\epsilon},k}} S^\alpha_{f,\tilde{\epsilon}}(\omega,t)d\omega\right] - A_k(t)\cos(2\pi\phi_k(t))\right| \leq C\tilde{\epsilon}$, where $C_\Psi = \int_0^\infty \frac{\overline{\hat{\Psi}(\xi)}}{\xi}d\xi$ and $B_{\tilde{\epsilon},k} := \{\omega,\ |\omega - \phi'_k(t)| < \tilde{\epsilon}\}$.

Remark: This version of the theorem differs slightly from the original since here we deal with real signals as opposed to complex; in addition, a different normalization of the WT is adopted from that originally proposed.

Component retrieval using the SST is thus first based on the computation of the *synchrosqueezing operator* $S^\alpha_{f,\tilde{\epsilon}}$ and then on its integration in the vicinity of curves defined by $\phi'_k(t)$.

D. Practical Implementation of the RCM in the SST Framework

We recall a practical implementation of the SST proposed by Brevdo et *al.* in [1] which is based on the theoretical results described above. To highlight the frequency components involved in the reconstruction of f, one defines a binning of the frequency $\{\omega_l\}_{l=0}^\infty$ and then $\mathcal{W}_l = [\frac{\omega_l+\omega_{l-1}}{2}, \frac{\omega_l+\omega_{l+1}}{2}]$. With this in mind, the synchrosqueezing operator $S^\alpha_{f,\tilde{\epsilon}}$ is approximated by: $T_f(\omega_l,t) = \int_{a:|\hat{\omega}(a,t)|\in\mathcal{W}_l} W_f(a,t)\frac{da}{a}$, which satisfies $f(t) = \frac{2}{C_\Psi}\mathcal{R}e\left[\sum_l T_f(\omega_l,t)\right]$.

By changing variables, we can write: $T_f(\omega_l,t) = \int_{u:|\hat{\omega}(2^{u/n_v}\Delta t,t)|\in\mathcal{W}_l} W_f(2^{u/n_v}\Delta t,t)\frac{\log(2)}{n_v}du$, where n_v is associated with the discretization of the scales a into $a_j = 2^{j/n_v}\Delta t$, $j = 0,\cdots,Ln_v-1$ and Δt being the time span. Now, putting $n_a = Ln_v$, the Nyquist-Shannon theorem suggests that the maximum frequency is $\bar{\omega} = \omega_{n_a-1} = \frac{1}{2\Delta t}$ and, under a periodic assumption for the signal, the minimum is $\underline{\omega} = \omega_0 = \frac{1}{T} = \frac{1}{n\Delta t}$ where $T = n\Delta t$ is the signal duration. Assuming ω varies on a log scale: $\omega_l = 2^{l\Delta\omega}\underline{\omega}$, we obtain $\Delta\omega = \frac{1}{n_a-1}\log_2(n/2)$. Consequently, for $t = q\Delta t$, a discrete version of $T_f(\omega_l, q\Delta t)$ can finally be written as follows:

$$T_{d,f}(\omega_l,q) = \sum_{0\leq j\leq n_a-1,\ j:|\hat{\omega}(a_j,q\Delta t)|\in\mathcal{W}_l} W_f(a_j,q\Delta t)\frac{\log(2)}{n_v}. \tag{7}$$

This operator satisfies $f(q\Delta t) \approx \frac{2}{C_\Psi}\mathcal{R}e\left[\sum_l T_{d,f}(\omega_l,q)\right]$. The strategy developed in [1] for the RCM is to proceed on a component by component basis. The idea is to find a curve $(c^*_q)_{q=0,\cdots,n-1}$, in the time-frequency plane such that it maximizes the energy while forces the modes to be smooth through a total variation term penalization and is obtained by computing the following quantity:

$$c^* = \underset{c\in\{0,\cdots,n_a-1\}^n}{\text{argmax}} \sum_{q=0}^{n-1}\log(|T_{d,f}(\omega_{c_q},q)|^2) - \sum_{q=1}^{n-1}\lambda\Delta\omega|c_q - c_{q-1}|^2. \tag{8}$$

Due to the complexity of the problem, only an approximation of c^* is sought using a greedy algorithm. In the sequel, we will use the implementation detailed in [2] of (8). When c^*_q has been found, the associated component at time $q\Delta t$ can be reconstructed by summing up $T_{d,f}(\omega_l,q)$ for l in $\mathcal{N}_q :=$

$[c_q^* - n_v/2, c_q^* + n_v/2]$ in the above formula. To find the next component, one sets $T_{d,f}(\omega_l, q)$ for $l \in \mathcal{N}_q$ to zero and restarts the minimization procedure on the remaining transform. In section IV-C, we will propose an alternative approach to this construction which will prove to be both more accurate and computationally much less demanding than the computation of c^*.

III. On the SST Parameters

In this section, we consider an analytic wavelet supported in $[\xi_\Psi - \Delta, \xi_\Psi + \Delta]$ in the Fourier domain. We first discuss the influence of the parameter Δ on the WT of signals made of pure harmonics and on that of a single ϵ-IMT. We then show that for a general multicomponent signal, it acts as a trade-off parameter that either favors the separation or the localization of the components in the time-scale space.

A. WT of Pure Harmonic Signals

The WT of a single tone $f(t) = A\cos(2\pi\phi t)$ is constant with time and equal to $W_f(a,t) = \frac{1}{2}Ae^{2i\pi\phi t}\overline{\hat{\Psi}(a\phi)}$, centered in $a = \frac{\xi_\Psi}{\phi}$. Its scale support is proportional to Δ since W_f is non zero only for a such that $\xi_\Psi - \Delta < a\phi < \xi_\Psi + \Delta \Leftrightarrow \frac{\xi_\Psi - \Delta}{\phi} < a < \frac{\xi_\Psi + \Delta}{\phi}$. When dealing with a signal made of pure harmonics $f(t) = \sum_{k=1}^{K} A_k \cos(2\pi\phi_k t)$, with $\phi_{k-1} < \phi_k$, the separation of the components using the WT is equivalent to the support of the WT of each component being disjoint that is for all $k > 1$:

$$\frac{\xi_\Psi + \Delta}{\phi_k} < \frac{\xi_\Psi - \Delta}{\phi_{k-1}} \Leftrightarrow \frac{\Delta}{\xi_\Psi} < \frac{\phi_k - \phi_{k-1}}{\phi_k + \phi_{k-1}}.$$

Finally, using the definition of the separation condition introduced in Definition 2, when $\Delta \leq \xi_\Psi d$ there is no interference between the components and $|W_f(a,t)| = \frac{1}{2}\sum_{k=1}^{K} A_k |\overline{\hat{\Psi}(a\phi_k)}|$.

B. WT of an ϵ-IMT

Let $f(t) = A(t)\cos(2\pi\phi(t))$ be a mode as defined in Definition 1, the WT of f is now approximated by:

$$W_f(a,t) \approx \frac{1}{2}A(t)e^{2i\pi\phi(t)}\overline{\hat{\Psi}(a\phi'(t))}, \tag{9}$$

the approximation error being controlled by $\epsilon(C_1(f)B_1 + C_2(f)B_2 + C_3(f)B_3)$ (see [5]), where C_i, $1 \leq i \leq 3$, does not depend on the wavelet choice, while $B_k := \int_{\mathbb{R}} |x|^k |\Psi(x)|\, dx$. So, when ϵ is high, a low approximation error requires that B_k must be small. One way to ensure this is to impose that Ψ has a fast decay or equivalently, that Δ be large.

C. WT of a Superposition of ϵ-IMTs

For a multicomponent signal $s(t) = \sum_{k=1}^{K} A_k(t)\cos(2\pi\phi_k(t))$ as defined in Definition 2, we wish to have the following kind of approximation:

$$W_f(a,t) \approx \sum_{k=1}^{K} \frac{1}{2} A_k(t) e^{2i\pi\phi_k(t)} \overline{\hat{\Psi}(a\phi_k'(t))}. \quad (10)$$

Following [5], this approximation error is again controlled by $\epsilon(\tilde{C}_1((f_i)_{i=1,\cdots,K})I_1 + \tilde{C}_2((f_i)_{i=1,\cdots,K})I_2 + \tilde{C}_3((f_i)_{i=1,\cdots,K})I_3)$, where $\tilde{C}_i$ does not depend on the wavelet choice. So, following the previous study on a single component, a low approximation error requires that Δ be large enough. Then, we also want each component to be well separated from the other components (which is compulsory if we are to use the WT for modes retrieval), that is for each (a,t) the sum in (10) should be reduced to a single term which is true provided that:

$$\frac{\xi_\Psi + \Delta}{\phi_k'(t)} < \frac{\xi_\Psi - \Delta}{\phi_{k-1}'(t)} \Leftrightarrow \frac{\Delta}{\xi_\Psi} < \frac{\phi_k'(t) - \phi_{k-1}'(t)}{\phi_k'(t) + \phi_{k-1}'(t)}.$$

Taking into account the separation condition (see Definition 2), we can deduce that the above inequality is true as soon as $\Delta < \xi_\Psi d$. To illustrate this, we consider successively a sum of two cosine functions with close frequencies and a sum of two linear chirps with close instantaneous frequencies, such that both signals satisfy the condition $\phi_1'(t) - \phi_2'(t) = \frac{1}{10}(\phi_1'(t) + \phi_2'(t))$. We analyze these signals with a bump wavelet (see (4)). We take $\xi_\Psi = \mu = 1$ and $\Delta = \sigma$ equal either to 0.2, 0.1 or 0.05. In Figure 1, we illustrate the trade-off role of the parameter Δ for the sum of two chirps, by drawing the magnitude of the WT (using a logarithmic basis in ordinate for the scales) for the two signals. The time span for the discretization of the signal is $\Delta t = 4/4095$, leading to 4096 sampling points and then the scales to compute the WT are defined, as in section II-D, by $a_j = 2^{j/n_v}\Delta t$, with $j = 0, \cdots, Ln_v - 1$, L being the dyadic length of f and n_v the number of scales per octave which we set to 32. It is clear that while the best result for the sum of cosines is obtained when σ is the smallest (Figure 1 C), for the sum of two chirps, none of the results are perfect, but the value $\sigma = 0.1$ realizes the best trade-off between the localization and the separation of the modes (Figure 1 E).

It is worth noting that the behavior of the SST was studied in detail in [8] for two tone signals. However, no conclusions can be drawn from the latter regarding modulated signals because the modulation considerably alters the wavelet representation of such signals and consequently the results given by the SST.

Remark: A very similar study was carried out by Mallat, ([14], p.102), but using a mother wavelet which was symmetric and compactly supported in the time domain. In such a case, the second order

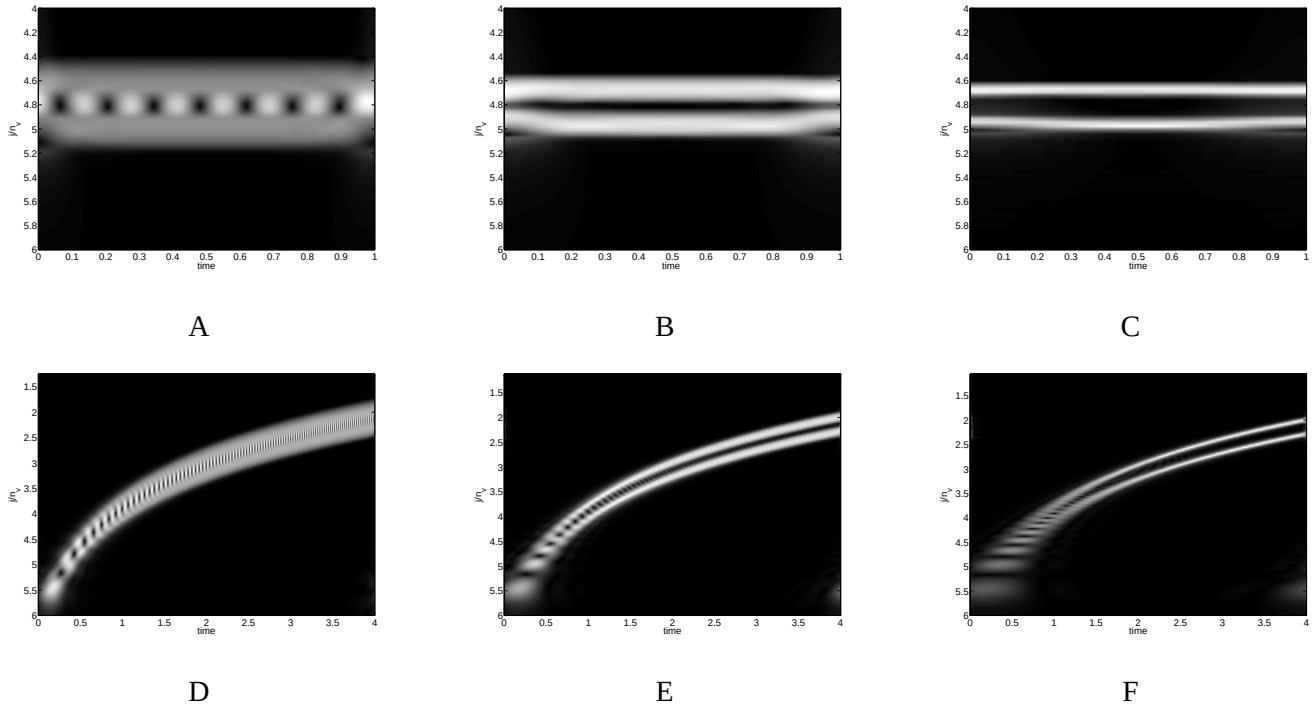

Fig. 1: From top to bottom: the modulus of the wavelet transform of the signal $\cos(80\pi t)+\cos(65.44\pi t)$, the modulus of the WT of $\cos(60\pi(t+1/4)^2)+\cos(49.10\pi(t+1/4)^2)$. The bump wavelet is used with parameters $\mu=1$ and from left to right: $\sigma=0.2,\,0.1,\,0.05$. The sampling rate is 4096 points over $[0,4]$ and $j/n_v=\log_2(\frac{a_j}{\Delta t})$

terms in the approximation (10) would be negligible only if for all k:

$$\frac{\xi_\Psi^2}{|\phi_k'(t)|^2}\frac{|A_k''(t)|}{|A_k(t)|}<<1 \text{ and } \xi_\Psi^2\frac{|\phi_k''(t)|}{|\phi_k'(t)|^2}<<1, \tag{11}$$

provided $\frac{\xi_\Psi}{|\phi_k'(t)|}\frac{|A_k'(t)|}{|A_k(t)|}\leq 1$. The second constraint of (11) when applied to an ϵ-IMT implies that ϕ_k is such that $\phi_k'(t)>>\xi_\Psi^2\epsilon$, provided that $\frac{\xi_\Psi}{|\phi_k'(t)|}\frac{|A_k'(t)|}{|A_k(t)|}\leq 1$, which is true when $\frac{\xi_\Psi\epsilon}{A_k(t)}\leq 1$, or equivalently $A_k(t)\geq\xi_\Psi\epsilon$. If we assume that both A_k and ϕ_k' are bounded below, the quality of the approximation (10) is all the better that ξ_Ψ is small when ϵ is large. Since one must also have $\Delta_\omega\leq\xi_\Psi d$ (where Δ_ω is the frequency bandwidth of the wavelet) to ensure separation of the different component, ξ_Ψ cannot be taken arbitrarily small. In contrast to the previous approach, the trade-off parameter between separation and localization of the components is now ξ_Ψ.

It is also worth noting that when no assumptions are made regarding the modulation parameter in the components of the signal, a general study provided in [17] relates the approximation (10) to the

derivatives of the Fourier transform of Ψ.

To conclude, the size of the frequency support of the mother wavelet plays a fundamental role when dealing with multicomponent signals ; adjusting this parameter enables us to tune between good separation and good localization of the modes.In the sequel we will use the previous remark regarding the size of the frequency support of the mother wavelet to build a new RCM algorithm.

IV. A New Algorithm for the Retrieval of Modes in a Synchrosqueezing Framework

Note that the matlab code corresponding to the implementation of the RCM algorithm we now propose is avalailable at [16]. This algorithm aims at identifying the ridge associated with each component from the magnitude of the WT and then reconstructing the components by using the information in the vicinity of the different ridges. It is based on three distinct steps: we first determine adaptively the number of modes, then we compute an optimal wavelet threshold which we finally use for retrieval of the modes.

A. Automatic Determination of the Number of Modes

Since, for a given time t, the scales $a_j = 2^{j/n_v}\Delta t$ of interest in the SST are those where $|W_f(a_j,t)|$ is large enough, we aim at detecting the modes using the following sets:

$$C_f(\gamma,t) = \{j, |W_f(a_j,t)| < \gamma \text{ and } |W_f(a_{j+1},t)| > \gamma\}. \tag{12}$$

Note that we could alternatively consider the set $\{j, |W_f(a_j,t)| > \gamma \text{ and } |W_f(a_{j+1},t)| < \gamma\}$. The natural expectation is that given t and when γ is appropriately chosen, each element of $C_f(\gamma,t)$ be associated with a single mode as defined in (12). We must also point out here that the normalization of the wavelet transform we use is necessary to give sense to the above set. Indeed, if we consider a sum of pure harmonics with the same amplitude then the wavelet transform at the frequencies of interest should also have the same amplitude. In our context and given γ, we will consider that a mode for a given time t is associated with a set of successive scales a_j such that $|W_f(a_j,t)| > \gamma$, and consequently with some index j_0 in $C_f(\gamma,t)$. With that in mind and given a range $\Gamma(t)$ for γ (the choice for $\Gamma(t)$ being discussed later on), we first compute an estimation of the number of modes at time t as follows:

$$M_f(t) \quad = \quad \underset{N}{\text{argmax}}\{\sum_{\gamma\in\Gamma(t)} \delta_{N,\#(C_f(\gamma,t))}\}$$

where $\#X$ denotes the cardinality of X and $\delta_{a,b} = 1$ if $a = b$ and0 otherwise. $M_f(t)$ indeed corresponds to the most frequent number of modes detected when γ varies in $\Gamma(t)$. We then define the number of

modes as follows:

$$N_f \quad = \quad \underset{N}{\text{argmax}}\{\sum_{t\in T}\delta_{N,M_f(t)}\}.$$

The quantity N_f corresponds to the most frequent number of modes over all times t and γ in $\Gamma(t)$. In what follows, we denote by $\Gamma(t)_{\min}$ and $\Gamma(t)_{\max}$ the lower and upper bounds for $\Gamma(t)$.

B. Wavelet Threshold

Once the number of modes is determined, we first consider the sets:

$$S_0(t) \quad = \quad \{\gamma \in \Gamma(t),\ \text{s.t. } \#(C_f(\gamma,t)) = N_f\}\,, \tag{13}$$

and define T_0 as the times t associated with non empty $S_0(t)$. A threshold $\hat{\gamma}(t)$ for the WT and t in T_0 is then computed as follows:

$$\hat{\gamma}(t) \quad = \quad \text{median}(S_0(t)). \tag{14}$$

It appears that, given t, $S_0(t)$ will be non empty provided that $a \rightarrow |W_f(a,t)|$ has at least N_f maxima and that $\Gamma(t)$ is appropriately chosen. Indeed, we have the following proposition:

Proposition 1: Assume that $a \rightarrow |W_f(a,t)|$ has N_f maxima located in (a^i) or that it has more than N_f maxima located in (a^i) and that $|W_f(a^i,t)| \neq |W_f(a^{i'},t)|$ if $i \neq i'$. If $\Gamma(t)_{\min} < \min_i |W_f(a^i,t)|$ and $\Gamma(t)_{\max} = \max_i |W_f(a^i,t)|$, then S_0 is non empty.

PROOF: Remarking that $a \rightarrow |W_f(a,t)|$ is continuous, if $a \rightarrow |W_f(a,t)|$ has exactly N_f maxima, there exists $\epsilon > 0$ such that $\gamma = \min_i |W_f(a_i,t)| - \epsilon$ is in $\Gamma(t)$ and $\#(C_f(\gamma,t) = N_f$ so that $S_0(t)$ is non empty. Now, if $a \rightarrow |W_f(a,t)|$ has more than N_f maxima, using the fact $|W_f(a^i,t)| \neq |W_f(a^{i'},t)|$ if $i \neq i'$ and the definition of $\Gamma(t)$ there exist γ_0 and γ_1 in $\Gamma(t)$ such that $\#(C_f(\gamma_0,t)) > N_f$ and $\#(C_f(\gamma_1,t)) \leq N_f$. As $|W_f(a^i,t)| \neq |W_f(a^{i'},t)|$ if $i \neq i'$, when γ varies from γ_0 to γ_1 there exists γ_2 such that $\#(C_f(\gamma_2,t)) = N_f$ and $S_0(t)$ is non empty ■.

Remark: The only time t where, whatever $\Gamma(t)$, $\hat{\gamma}(t)$ will not be defined is when $a \rightarrow |W_f(a,t)|$ has less than N_f maxima. These times will be discarded in the RCM algorithm whose description follows.

C. Algorithm for Modes Retrieval

For a time $t \in T_0$, we successively define $\#C_f(\hat{\gamma}(t), t)$ sets of integers $I_k(t)$, $1 \leq k \leq \#C_f(\hat{\gamma}(t), t)$, as follows:

$$\begin{cases} I_k(t) = \{j_k(t), \cdots, J_k(t)\} \; s.t. \; \forall j_k(t) \leq j \leq J_k(t) \; |W_f(a_j, t)| > \hat{\gamma}(t) \\ |W_f(a_{j_k(t)-1}, t)| < \hat{\gamma}(t) \text{ and } |W_f(a_{J_k(t)+1}, t)| < \hat{\gamma}(t), \\ j_k(t) < j_{k+1}(t). \end{cases}$$

Each set $I_k(t)$ is made of indices corresponding to some scales of interest which can be associated with one of the modes when $t \in T_0$ (because $\#C_f(\hat{\gamma}(t), t) = N_f$ in that case). The RCM algorithm is then straight forward. We consider for each t in T_0 the set $I_{N_f-k+1}(t)$, which enables us to retrieve the mode k by applying the following approximation formula:

$$f_k(t) \approx \frac{2}{C_\Psi} \mathcal{R}e \left[\sum_{j \in I_{N_f-k+1}(t)} W_f(a_j, t) \frac{\log(2)}{n_v} \right]. \tag{15}$$

Note that the index of I in the sum comes from the fact that I_k for small k corresponds to high frequency component and that in Definition (2) the components are arranged in increasing frequency order.

Doing so, we avoid both the problem of the binning of the frequency domain as well as the heuristic procedure involved in the determination of the modes (see section II-D). Furthermore, this reconstruction procedure is fully automatic and avoids the need to narrow down the curve searching in the time-scale space before proceeding with the mode retrieval [1]. As already mentioned, the threshold $\hat{\gamma}(t)$ is computed to ensure good detection of the different modes. However reconstructing the modes using such a threshold leads to some large amplitude wavelet coefficients being neglected. To improve the reconstruction, we comment that since $\hat{\Psi}$ is compactly supported inside $[\xi_\Psi - \Delta, \xi_\Psi + \Delta]$, then basically the scales of interest for the component k at time t are $[\frac{\xi_\Psi - \Delta}{\phi_k'(t)}, \frac{\xi_\Psi + \Delta}{\phi_k'(t)}]$. Invoking (9), the amplitude of the WT attains a local maximum when $a_j \phi_k'(t) = \xi_\Psi$. A good estimation $\bar{\phi}_k'(t)$ of $\phi_k'(t)$ is obtained by considering, for t in T_0, $\frac{\xi_\Psi}{a_{j_0}}$ where $a_{j_0} := \underset{a_j}{\text{argmax}} \left\{ |W(a_j, t)|, j_{N_f-k+1} \leq j \leq J_{N_f-k+1} \right\}$. The reason for considering $N_f - k + 1$ instead of k is again related to the fact that the modes should be arranged in increasing frequency order. This finally leads us to an alternative approximation formula (for t in T_0):

$$f_k(t) \approx \frac{2}{C_\Psi} \mathcal{R}e \left[\sum_{a_j \in L_k(t)} W_f(a_j, t) \frac{\log(2)}{n_v} \right], \tag{16}$$

where $L_k(t) = [\frac{\xi_\Psi - \Delta}{\phi_k'(t)}, \frac{\xi_\Psi + \Delta}{\phi_k'(t)}]$. We investigate in the next section the relevance of the reconstruction formula (16) and we will also put forward its potential interest for signal sampling and denoising in

section VI.We should finally mention that the computational cost of the algorithm is essentially related to the cost of the steps described in sections IV-A and IV-B: for each time t we compare the modulus of the WT computed at Ln_v scales with $\#\Gamma(t)$ thresholds (an upper bound of the computational cost is thus $\max_t \#\Gamma(t) \times Ln_v \times n$, $T = n\Delta t$ being the total duration of the signal).

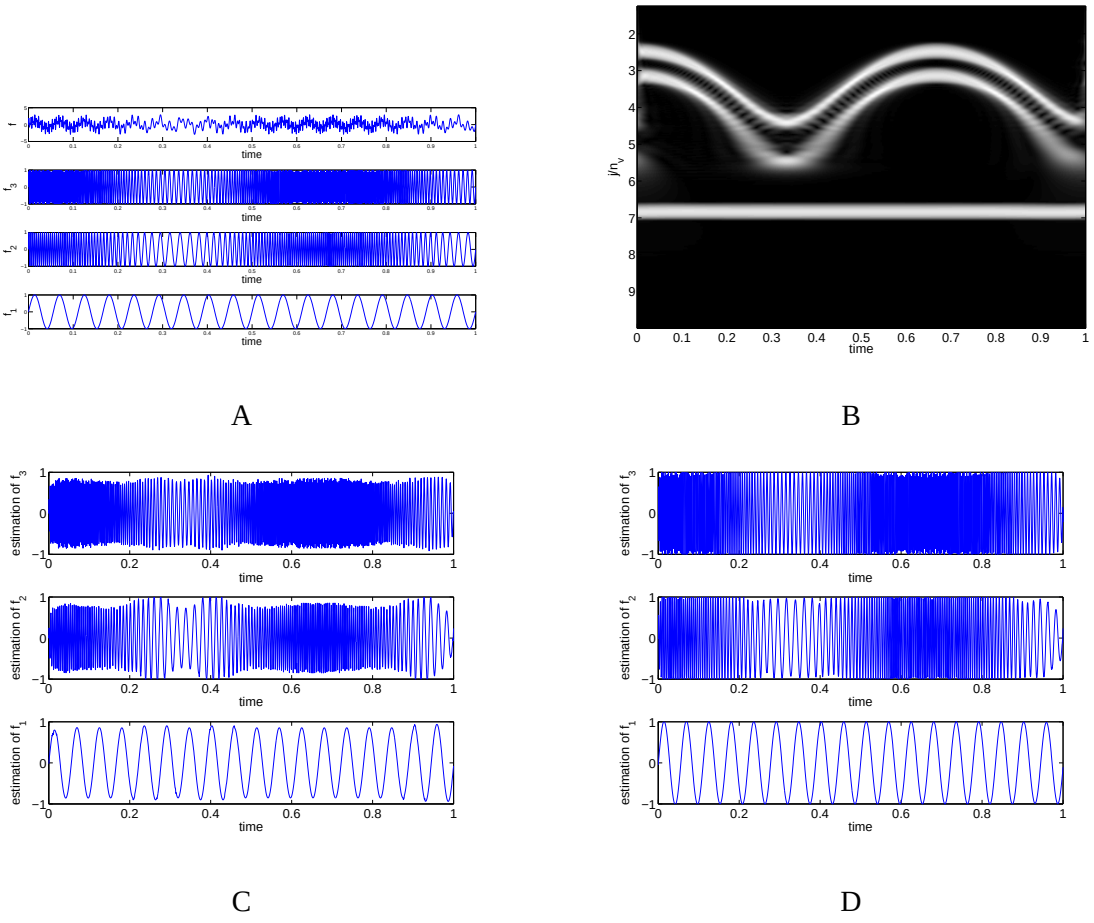

Fig. 2: A: An example of a signal made of the superposition of non trivial IMTs ; B: modulus of the corresponding WT ; C: reconstruction of the modes of the signal in A using formula (15) and the bump wavelet ($\mu = 1$ and $\sigma = 0.2$) ; D: same as in C but using the reconstruction formula (16).

V. Illustrations of the Reconstruction Procedure and Comparisons

In this section, we compare some examples to illustrate the advantage of using the reconstruction approach described above as opposed to that proposed in section II-D and implemented in [1]. Furthermore, we will compare the proposed method to EMD which extracts the modes by analyzing the

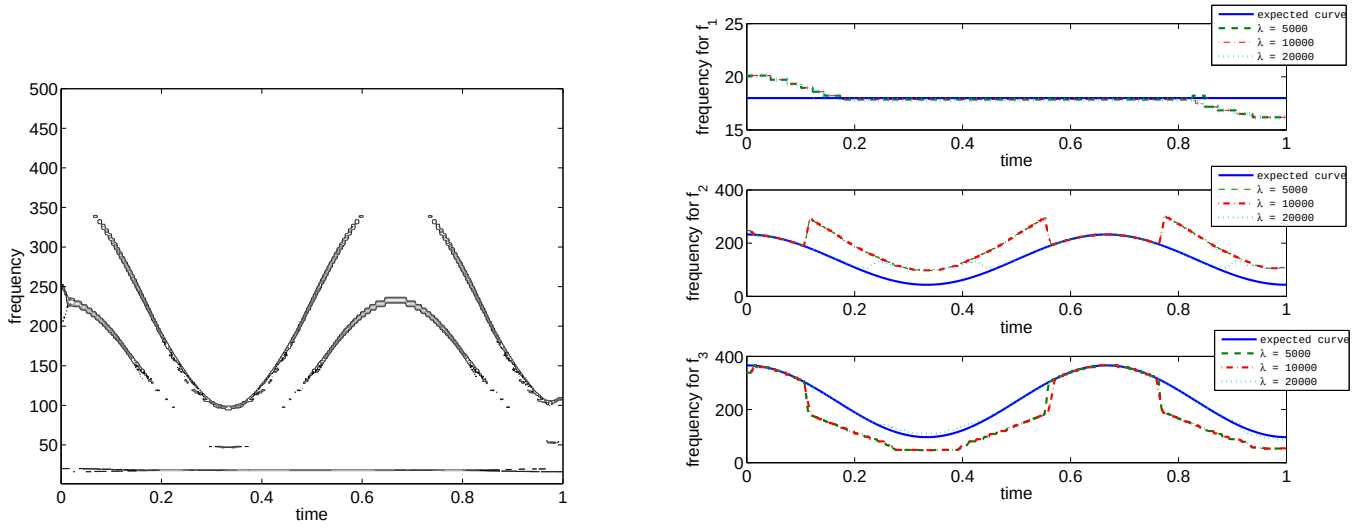

A B

Fig. 3: A: Contour plot of the modulus of the absolute value of $T_{d,f}$ associated with the signal of Figure 2 A. B: The curves c^*, for different values of λ for the studied signal along with the expected curve. From top to bottom: the curves associated with modes f_1, f_2 and f_3.

signal in the time domain [11]. In the simulations of this section, the set $\Gamma(t)$ will be a discretization of $[10^{-2}, \max_a |W_f(a,t)|]$ (the discretization step being set to 10^{-3}).

A. Analysis of Frequency Modulated Multicomponent Signals

To illustrate the reconstruction procedure defined in (15) and (16), we consider the retrieval of the components of a modulated frequency signal $f(t) = f_1(t) + f_2(t) + f_3(t)$ with $f_1(t) = \sin(3(2\pi \times 6t)$, $f_2(t) = \sin(3(2\pi \times 46t + 21\sin(3\pi t)))$ and $f_3(t) = \sin(3(2\pi \times 77t + 30\sin(3\pi t)))$ (see Figure 2 A), which has a frequency separation condition $d \approx 0.2$ (see Definition 2). The studied signal is made of 2048 equi-spaced samples on $[0, 1]$ and admits the WT whose modulus is displayed on Figure 2 B computed using the bump wavelet with $\mu = 1$ and $\sigma = 0.2$. The representation uses a logarithmic basis for the discretized scales $a_j = 2^{j/n_v}\Delta t$,$j =), \cdots, Ln_v$ (n_v and L being defined as previously), i.e. $j/n_v = \log_2(a_j/\Delta t)$. We test the two reconstruction methods (15) and (16) on the signal with the results depicted in Figure 2 C and D respectively. To measure quantitatively the improvement in terms of mode retrieval brought about by the use of the second method over the first one, we compute the SNR (measured in Decibels

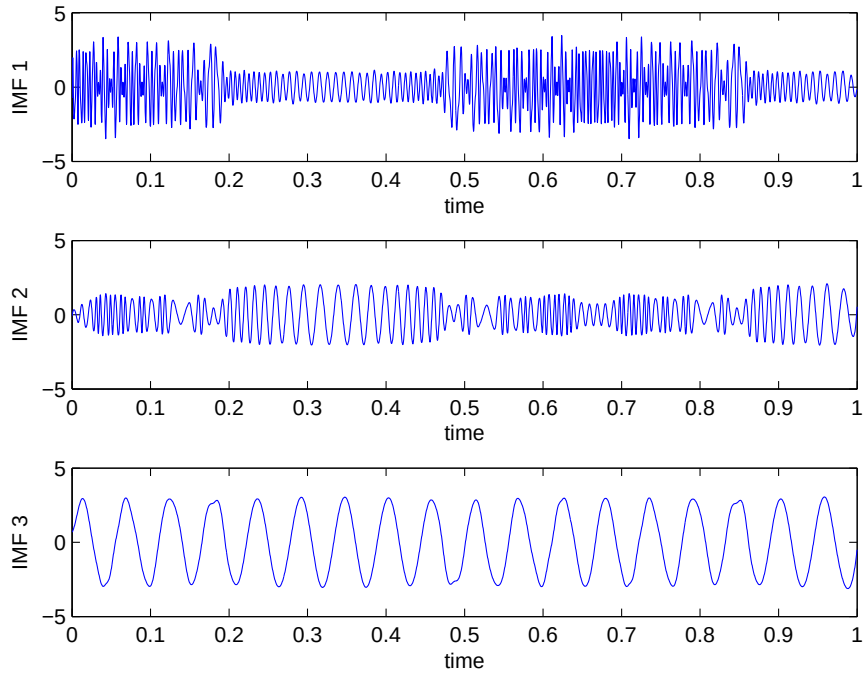

Fig. 4: The results of the EMD decomposition on the signal of Figure 2 A.

(dB)) defined as follows:

$$SNR \quad = \quad 10\log_{10}(\frac{\|f_i\|_2^2}{\|\tilde{f}_i - f_i\|_2^2}), \tag{17}$$

for each f_i, $i = 1, 2, 3$ and $\tilde{f}_i$ being the estimate. The SNR corresponding to f_1, f_2 and f_3 of Figure 2 A is 19.1 dB, 11.6 dB and 13.6 dB for (15) and 31.7 dB , 14.5 dB and 22 dB for (16). A careful look at Figure 2 D shows that a better restoration of the amplitude of the modes is achieved using formula (16) (for instance, compare Figure 2 C and D betweentimes 0.3 and 0.4). Finally, we should mention that we have noticed that when the parameters σ and μ are correctly set in accordance with the separation condition d, using a much larger discretization step for $\Gamma(t)$ (typically 10^{-2} instead of 10^{-3}) does not alter the reconstruction performance.

Now, we wish to compare the procedure we proposed for reconstruction to that introduced in section II-D. First, we remark that formula (8) proposed to determine the curves c^* before reconstruction requires the knowledge of the number of modes. We aim to show that even if the latter is known, this determination may be inaccurate. To ensure a fair comparison, we run the implementation available in [2] of formula

(8) for the signal of Figure 2 A using the bump wavelet still with $\mu = 1$ and $\sigma = 0.2$, and then display the curves $c*$ depending on the value of λ and the expected one on Figure 3 B (the tested values are $\lambda = 5.10^3$, 10^4 and 2.10^4). We also display the contour plot associated with the modulus of $T_{d,f}$ on Figure 3 A.

From this last Figure, it is clear that to determine the curves c^* only based on the modulus of $T_{d,f}$ leads to an accurate curve c^* associated to f_2 because the modulus of $T_{d,f}$ is much too low in the vicinity of the expected curve: this motivates the use of the regularization parameter λ. Indeed, consideration of Figure 3 B is very informative in this regard. For a smaller λ, the curves c^* given by (8) are made of several parts that belong to different frequency bands because the synchrosqueezing part prevails in (8), i.e. it creates mode-mixing. Taking a larger λ enables to compensate for the small modulus of $T_{d,f}$ since the regularization term then prevails over the synchrosqueezing term in (8). Nevertheless, however high the value for λ is, one cannot retrieve the expected curves and, eventually, if λ is taken too large one ends up with some c^* being straight lines. As a result of this inaccuracy in the determination of the curves c^*, the reconstruction algorithm based on these curves (see the end of section II-D) is inefficient in such a case.

Another technique used to represent such signals is EMD [11]. The main principle of the technique is to extract components which are less and less oscillatory from a signal by applying an iterative procedure called the sifting process (for further details on the method see [11]). We applied the EMD to the signal of Figure 2 A using the versions given in [18] or in [12] with the default parameters in each case. The components of the decomposition, called IMFs (intrinsic mode functions), sum up to the original signal. In the EMD context, IMF_k for small k corresponds to a high frequency component. We display on Figure 4 the decomposition given by the implementation of [12] of the EMD (the other leading to very similar results). We notice some mode-mixing between IMF_1 and IMF_2. The reason for such mode-mixing effects is related to the fact that the extraction of the IMFs in the EMD is not frequency based in contrast with the synchrosqueezing technique. Furthermore, we also comment that if an error is made in the extraction of the first IMF then it will spread throughout the whole extraction procedure. A deeper analysis of Figure 3 tends to show that when the real modes are well separated (meaning that $\frac{\phi'_k(t)-\phi'_{k-1}(t)}{\phi'_k(t)+\phi'_{k-1}(t)} >> d$, typically for $0.2 < t < 0.45$) the EMD enables a good separation, the extraction being more difficult in the opposite case. It is worth noting that for such a signal a good separation of the modes would be possible using the EMD but would require an astronomical number of sifting iterations (approximately 20000). We would note that recent developments were proposed in [10] [21] which aim to redefine EMD to better handle the mode-mixing effect induced in the original algorithm.

B. Analysis of Linear Chirp

In this section, we provide another illustration of the method on the extraction of linear chirps. Our aim is on the one hand to compare the behavior of our method with existing methods, namely EMD [11] and another version of the RCM based on the SST [1] and also to focus on the importance of the mother wavelet choice in the synchrosqueezing technique when ϵ is large.

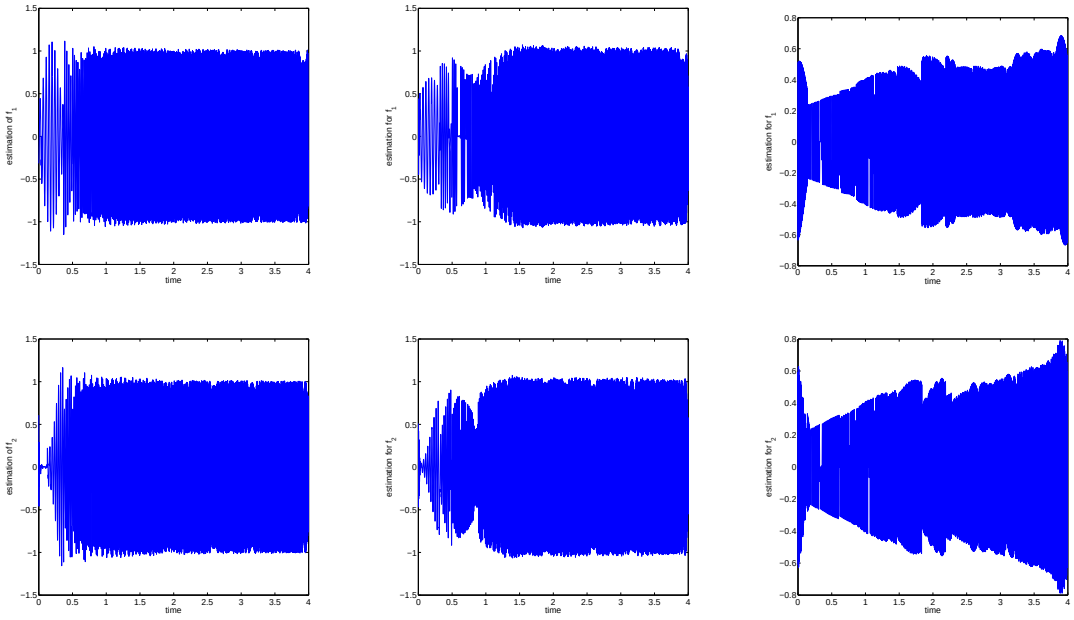

Fig. 5: The first row contains the estimation of f_1 using the reconstruction formula (16) with the wavelet the bump wavelet with $\mu = 1$ and $\sigma = 0.1$ and$\sigma = 0.05$, $\sigma = 0.01$ from left to right. The second row contains the estimation of f_2 with the same parameters with regards to the WT

To do so, we analyze the linear chirp signal $f(t) = f_1(t) + f_2(t)$ with $f_1(t) = \cos(49.1\pi(t + 1/4)^2)$ and $f_2(t) = \cos(60\pi(t + 1/4)^2)$, whose WT was explored in Figure 1. The second row of Figure 1 showed the importance of the parameter $\sigma = \Delta$, the radius of the support of the Fourier transform of the wavelet, in terms of the quality of the representation. We now remark that the WT associated with the bump wavelet (see (4)) defined by the set of $(r\mu, r\sigma)$ is the same as that obtained taking (μ, σ) except that the scales are dilated by a factor of r. Thus, not changing the amplitude of the wavelet transform, does not alter the behavior of our RCM algorithm. So, without any loss of generality μ can be set to 1, σ being the only parameter that may vary.

In the present case, since $d = 1/10$ and since μ is taken equal to 1, the maximum value for $\Delta = \sigma$ should be 0.1. Now, we show the importance of choosing σ as close as possible to this upper bound for mode retrieval. We use the reconstruction formula (16) as suggested by the previous simulations on frequency modulated multicomponent signals again using the bump wavelet for analysis. Our simulations consider the value 0.1, 0.05 and 0.01 for σ.

The results of Figure 5 show that by improving the accuracy of approximation (9), the mode retrieval procedure works much better. Note that when the reconstruction formula returns zero, i.e. $t \notin T_0$, this means that our algorithm is not able to separate the mode from the wavelet representation and we find it wiser not to propose any decomposition in such cases: when the analysis tools are inefficient this should be explicit. The rationale underlying this view is to make the most of the wavelet decomposition without extrapolating when the information is unclear. To measure quantitatively the improvement in terms of mode retrieval brought about by the variation on σ, we compute, for the time indices such that $t > 0.8$, the SNR (measured in Decibels (dB), see (17)) associated with the retrieval of f_i, $i = 1, 2$.

	$\sigma = 0.1$ $\mu = 1$ $t > 0.8$	$\sigma = 0.05$ $\mu = 1$ $t > 0.8$	$\sigma = 0.01$ $\mu = 1$ $t > 0.8$
SNR (in dB,f_1 estimate)	20.8	14	1.2
SNR (in dB,f_2 estimate)	24	14.5	1.6

TABLE I: Influence of the parameter σ on the mode retrieval procedure

The results (depicted in Table I) confirm our basic insight that better reconstruction is achieved for smaller times by moving σ closer to its upper bound given by the separation condition. Note also that to take a larger σ worsens the wavelet representation for large t in the sense that its spreads the information over a larger number of scales. However, for these t, since the reconstruction procedure is basically a summation over scales given by the wavelet support, to take a larger σ has no impact on the quality of the estimation of the modes. Finally, we again notice that when the parameters μ and σ are set according to the separation condition, taking a much larger discretization step for the set $\Gamma(t)$ (typically 10^{-2} instead of 10^{-3}) does not alter the reconstruction performance.

We are also concerned with comparing our method for mode extraction to the EMD and to the technique of extraction of the modes given by (8). For EMD, the useful information is mainly contained in the

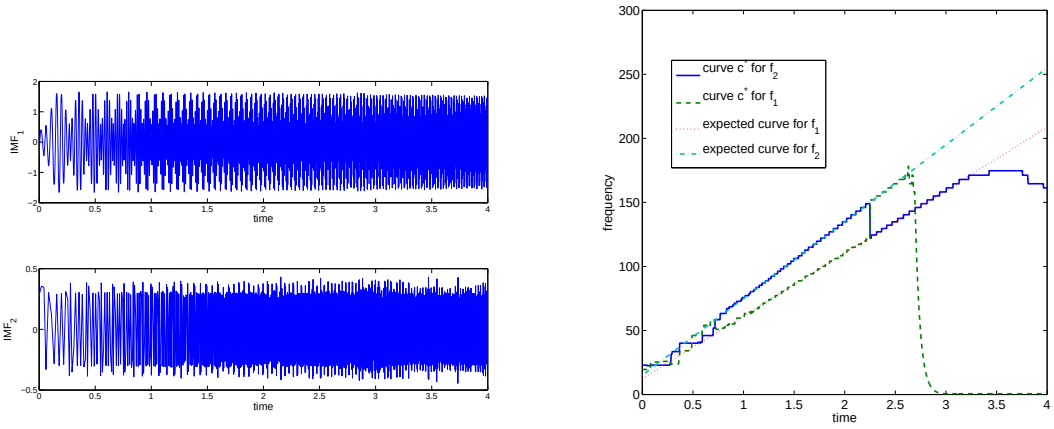

A B

Fig. 6: A: The first two IMFs associated with the decomposition of the linear chirp ; B: The curves c^* given by the formula (8) with $\lambda = 1000$ along with the expected curves

first two IMFs, which are displayed in Figure 6 A. The reconstruction error (measured in dB) is for the first and second modes (considering times larger than $t > 0.8$ to ensure a fair comparison with the synchrosqueezing technique) 2.09 dB and 2 dB respectively. Again, as the EMD does not analyze the signal in the frequency domain it seems to be inefficient at separating components with close frequency characteristics. We finally investigate how the curve seeking procedure given by formula (8) works on the studied signal. To do so, we consider the decomposition of the linear chirp signal with the bump wavelet taking $\mu = 1$ and $\sigma = 0.1$, the parameter λ for curve seeking is set to 1000. Again we notice that the formula (8) for curve seeking results in mode-mixing (to display the corresponding modes is then worthless), other values of λ would offer no improvement.

VI. Application of the RCM to Signal Non-Uniform Sampling and Denoising

A. Application of the RCM to Multicomponent Signals Non-Uniform Sampling

In this section, we investigate the potential interest of the RCM for efficient non-uniform sampling of multicomponent signals. Let us define g as the cubic spline interpolant of f at the sample points (t_m). Then if $D = \max_m |t_{m+1} - t_m|$, the interpolation error e satisfies $\|e\|_{L^\infty} \leq \frac{5}{584} D^4 \|f^{(4)}\|_{L^\infty}$. Note that if g were defined using a piecewise cubic Hermite interpolant instead, we would have: $\|e\|_{L^\infty} \leq \frac{1}{384} D^4 \|f^{(4)}\|_{L^\infty}$, which suggests that, given a set of samples $(t_m, f(t_m)))$, a lower interpolation error should be achieved

by using a piecewise cubic interpolant. However, writing the upper bound of the error as previously wipes out the locality of the error estimation. Indeed, we write the following when the piecewise cubic interpolant is used [9]:

$$\|e\|_{L^\infty} \leq \frac{1}{384} \max_m \left\{ (t_{m+1} - t_m)^4 \|f^{(4)}\|_{L^\infty,[t_m,t_{m+1}]} \right\}, \tag{18}$$

where $\|.\|_{L^\infty,[t_m,t_{m+1}]}$ stands for the supremum on the interval $[t_m, t_{m+1}]$. This means that where $f^{(4)}$ is large, the sample points t_m and t_{m+1} should be close.

To adaptively choose non-uniform samples to minimize the interpolation error is a thorny issue. A method inspired by the EMD consists of selecting the extrema of the signal, such that they depend locally on the strength of the oscillations. Another possibility would be to choose equi-spaced sample points over the whole signal duration.

We seek to show that the location of the extrema of the high frequency component obtained after applying our RCM algorithm are more relevant as sample points for f than the locations of the extrema of the signal itself. The result will be measured in terms of the magnitude of the error e. Indeed, let us consider the following three signal reconstruction procedures. The first (resp. second) one consists of considering as non-uniform sample points for f the location of the extrema of the high frequency mode given by the RCM we propose (resp. of the original signal) and then piecewise cubic Hermite interpolation of f at these points. The third approach follows the same framework as the first two, the sample points being equi-spaced with the same average sampling rate. We display in Figure 7, the interpolation errors associated with the three different cases (the number of interpolation points being the same in each case) for the signal defined in Figure 2 A. Note that by choosing the sample points as the location of the extrema of the high frequency component obtained with our RCM algorithm, we manage to significantly reduce the interpolation error compared to the other two methods. Figure 7 C shows that to maintain that error at a low level, the sample points have to be chosen according to the frequency content of the signal.

B. Sensitivity to Sampling of the RCM Algorithm

We now investigate the sensitivity of the RCM we propose to sampling. For that purpose, given a set of non-uniform signal samples, we compute the RCM of the interpolating signal (using again the piecewise Hermite interpolant) and compare it with the RCM of the signal itself. To quantify the error we make when computing the RCM on the signal interpolant, we compute for each mode the SNR corresponding to the discrepancy between the mode computed using the whole signal and that computed using different

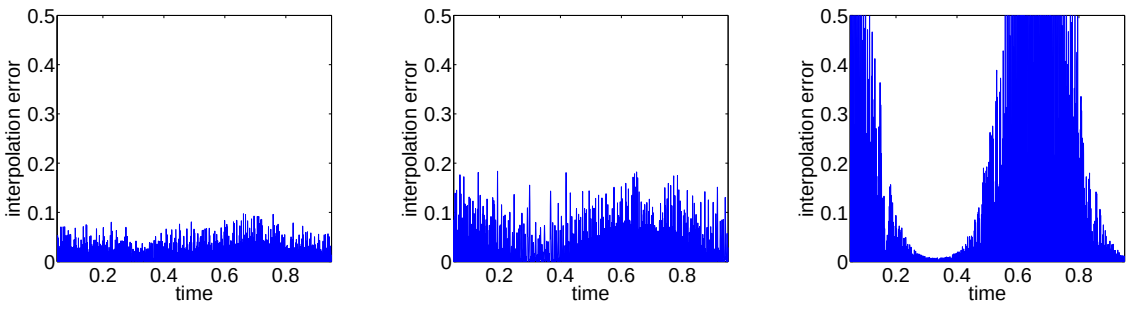

Fig. 7: A: display of the interpolation error of the signal of Figure 2 A where (t_m) are the location of the extrema of the high frequency mode obtained with our RCM algorithm ; B: same computation where (t_m) are the location of extrema of the signal f ; C: same computation when the sample points are equi-spaced on $[0, 1]$. The number of sample points equals 462 in each case.

kinds of sample points. As previously, we compare the results of the RCM when the sample points are either equi-spaced, the location of the extrema of the signal or that of the high frequency mode. Table II summarizes the results still for the signal f of Figure 2 A and shows that the RCM is much more accurate when the sample points are the extrema of the high frequency mode. Bearing in mind the previous study, this suggests that the accuracy of the RCM applied to the interpolating signal of at non-uniform samples is directly related to the interpolation error. The investigation into the theoretical reasons why the algorithm behaves this way is the subject of further research which we will report subsequently.

	Uniform	Extrema of f	Extrema of high frequency mode
SNR (in dB, f_1 estimate)	12.4	26.3	30
SNR (in dB, f_2 estimate)	18.6	27.5	30.4
SNR (in dB, f_3 estimate)	37	43.1	51.3

TABLE II: SNR associated with RCM based on signal interpolants versus RCM based on the original signal, for different sets of sample points.

C. Sensitivity to Noise, Denoising Algorithm

In this subsection we show that the RCM enables us to define a denoising algorithm that outperforms the wavelet denoising technique for a wide range of noise level.

When dealing with noise, we must take into account the noise level in the determination of $\Gamma(t)$. We do not change the value for $\Gamma(t)_{\max}$ which still equals $\max_a |W_f(a,t)|$, but to determine the lower bound for $\Gamma(t)$ we proceed as follows. Assume the standard deviation of the noise η is known, taking into account (9) which divides the amplitude of the original signal by $1/2$, it is natural to take into account only the coefficients that are above $\frac{\eta}{2}$. To estimate the standard deviation of the noise, we use a robust estimator $\bar{\eta}$ of η based on the finest detail coefficients of an orthogonal wavelet decomposition [14] (in our simulations, we have used the symmlet with 4 vanishing moments, changing the number of vanishing moments does not change the estimate a great deal). The lower bound for $\Gamma(t)$ is finally set to $\Gamma(t)_{\min} = \frac{\bar{\eta}}{2}$.

Our point is to show that the RCM algorithm we have proposed is an efficient tool for the denoising of multicomponent signals. We again consider the multicomponent signal which we previously studied for signal interpolation to which we add a Gaussian white noise. Using different standard deviations for the noise, we obtain SNRs before denoising between the original and noisy signals. Then, we apply our RCM to the noisy signal (still considering the bump wavelet with $\mu = 1$ and $\sigma = 0.2$ as in the noise-free case) and we obtain the so-called denoised signal by summing up all the obtained modes. We finally compute the SNR after denoising between the denoised and the original signals and plot these in Figure 8 versus the SNR before denoising (curve labelled RCM on that Figure). We now compare the behavior of the RCM algorithm in terms of denoising to two other wavelet thresholding techniques: the translation invariant hard wavelet thresholding [6] and the block thresholding technique proposed in [15].

The results depicted on Figure 8 clearly show that the block thresholding technique and the denoising technique based on the RCM we propose behave much better than the traditional translation invariant wavelet thresholding (TIWT). The main reason for that behavior is that the first two methods are basically time-frequency like tools, while the TIWT is well suited for signals containing singularities. We also believe that our algorithm behaves better than the TIWT for the reason that the threshold applied to the wavelet coefficients in the latter technique is computed depending on the octave the coefficients belong to, whereas the threshold in the RCM method is adapted for each time t depending on the number of modes found. The comparison of our method with the block thresholding (BT) method shows better behavior for SNRs between 6 and 12 dB. For a high SNR, our method behaves worse than the BT mainly because

the approximation (9) becomes too crude. For a low SNR our method behaves worse than the BT as soon as the correct number of modes is not found (typically in that case for a SNR smaller than 5 dB). In future work, we will address this issue by seeking to take into account second order terms in (9) to better handle the denoising of signal when the SNR is high.

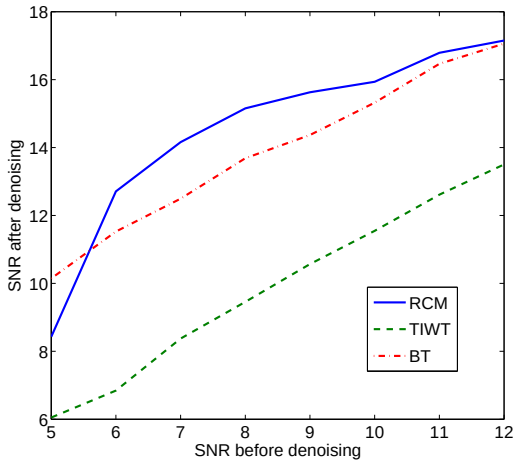

Fig. 8: SNR after denoising as a function of the SNR before denoising either using the RCM technique we propose (RCM), the translation invariant wavelet thresholding (TIWT) or the block thresholding (BT)

ACKNOWLEDGEMENT

The authors would like to thank the reviewers for their useful comments which helped improve the general presentation of the paper.

VII. CONCLUSION

In this paper, we have presented a novel algorithm for the retrieval of the components of a multicomponent signal based on some ideas exploited by the synchrosqueezing transform. After emphasising the importance of the accuracy of the wavelet representation for so-called ϵ-IMTs, we then profited from the structure of the wavelet transform of multicomponent signals to develop a novel algorithm for retrieving the component of these signals. We then showed that with regard to the mode-mixing issue,the proposed algorithm behaves better than EMD or another existing implementation of mode retrieval based on the synchrosqueezing method. We then showed that in the noise-free configuration, the proposed algorithm

can be used to find out an appropriate sampling of multicomponent signals which ensures the stability to the mode retrieval algorithm we proposed. Finally we showed that the algorithm also provides a natural way to denoise multicomponent signals which outperforms, for a wide range of SNRs, the most up-to-date time-frequency denoising algorithm based on block-thresholding. Future work requires a deeper theoretical study of the component retrieval algorithm we proposed along with some new developments on synchrosqueezing-like techniques, especially by working on better approximations of the wavelet representation.

REFERENCES

[1] E. Brevdo, N. S. Fuckar, G. Thakur, H-T. Wu, *The Synchrosqueezing Algorithm: a Robust Analysis Tool for Signals with Time-Varying Spectrum,* submitted, 2011, arXiv id: 1105.0010.

[2] https://web.math.princeton.edu/ebrevdo/synsq/

[3] R. A. Carmona, W.L. Hwang, and B. Torrésani, *Multiridge Detection and Time-Frequency Reconstruction,* IEEE Transactions on Signal Processing, vol. 47, no. 2, pp. 480-492, 1999.

[4] E. Chassande-Mottin, I. Daubechies, F. Auger and P. Flandrin, *Differential Reassignment,* IEEE Signal Processing Letters, vol. 4, no. 10, pp. 293-294, 1997.

[5] I. Daubechies, J. Lu and H-L. Wu, *Synchrosqueezed Wavelet Transforms: an Empirical Mode Decomposition-Like Tool,* Applied and Computational Harmonic Analysis, vol. 20, no. 2, pp. 243-261, 2011.

[6] D. L. Donoho,I. M. Johnstone, *Ideal Spatial Adaptation by Wavelet Shrinkage,* Biometrika, vol. 81, pp. 425-455, 1994.

[7] P. Flandrin and P. Borgnat, *Time-Fequency Energy Distributions Meet Compressed Sensing,* IEEE Transactions on Signal Processing, vol. 58, no. 6, pp. 2974-2982, 2010.

[8] H-T. Wu, P. Flandrin and I. Daubechies, *One or Two Frequencies? The Synchrosqueezing Answer,* Advances in Adaptive Data Analysis, vol. 3, no.1-2, pp. 29-39, 2011.

[9] Hildebrand, F. B. *Introduction to Numerical Analysis,* New York: McGraw-Hill, pp. 314-319, 1956.

[10] X. Hu, S. Peng, and W-L. Hwang, *EMD Revisited: A New Understanding of the Envelope and Resolving the Mode-Mixing Problem in AM-FM Signals,* IEEE Transactions on Signal Processing, vol.60, no. 6, pp. 1075-1086, 2012.

[11] N.E. Huang, Z. Shen, S.R. Long, M.C. Wu, H.H. Shin, Q. Zheng, N-C. Yen, C. C. Tung and H.H. Liu, *The Empirical Mode Decomposition and Hilbert Spectrum for Nonlinear and Non-Stationary Time Series Analysis,* Proceedings of the Royal Society of London, vol. 454, pp. 903-995, 1998.

[12] http://rcada.ncu.edu.tw/research1_clip_program.html

[13] J.M. Lilly and S.C. Olhede, *On the Analytic Wavelet Transform,* IEEE Transactions on Information Theory, vol. 56, no. 8, pp. 4135-4156, 2010.

[14] S. Mallat, *A Wavelet Tour on Signal Processing,* Academic Press, 1998.

[15] G. Yu, S. Mallat, and E. Bacry, *Audio Denoising by Time-Frequency Block Thresholding,* IEEE Transactions on Signal Processing, vol. 56, no. 5, pp. 1830-1839,2008.

[16] http://www-ljk.imag.fr/membres/Sylvain.Meignen/recherche/index.html

[17] S. Olhede and A.T. Walden, *The Hilbert Spectrum via Wavelet Projections,* Proc. R. Soc. Lond. A, vol. 460, pp. 955-975, 2004.

[18] G. Rilling, P. Flandrin and P. Goncalves, *On Empirical Mode Decomposition and its Algorithms,* IEEE-EURASIP Workshop on Nonlinear Signal and Image Processing, NSIP-03, Grado (I), June 2003.

[19] X. Rodet and P. Depalle, *A New Additive Synthesis Method Using Inverse Fourier Transform and Spectral Envelope,* In Proc. ICMC, San Jose, 1992.

[20] G. Thakur and H-T. Wu, *Synchrosqueezing-Based Recovery of Instantaneous Frequency from Nonuniform Samples,* SIAM J. Math. Analysis, vol.43, no. 5, pp. 2078-2095, 2011.

[21] Z. Wu and N-E. Huang, *Ensemble Empirical Mode Decomposition: A Noise-Assisted Data Analysis Method,* Advances in Adaptive Data Analysis, vol.1, no. 1, pp. 1-41, 2009.